LAWRENCE
LIVERMORE
NATIONAL
LABORATORY

LLNL-TR-417646

Mechanical Properties of Unreinforced Brick Masonry, Section1

K. Mosalam, L. Glascoe, J. Bernier

October 7, 2009

This work performed under the auspices of the U.S. Department of Energy by Lawrence Livermore National Laboratory under Contract DE-AC52-07NA27344.

Executive Summary

Before the advent of concrete and steel, masonry helped build civilizations. From Egypt in Africa, Rome in Europe, Maya in the America to China in Asia, masonry was exploited to construct the most significant, magnificent and long lasting structures on the Earth. Looking at the Egyptian pyramids, Mayan temples, Roman coliseum and Chinese Great Wall, one cannot stop wondering about the significance and popularity that masonry has had through out history. Lourenco et al (1989) summed up the reasons for the popularity of masonry in the following,

> *"The most important characteristic of masonry construction is its simplicity. Laying pieces of stone or bricks on top of each other, either with or without cohesion via mortar, is a simple, though adequate, technique that has been successful ever since remote ages. Other important characteristics are the aesthetics, solidity, durability, low maintenance, versatility, sound absorption and fire protection."*

Despite these advantages, masonry is no longer preferred structural material in many parts of the developed world, especially in seismically active parts of the world. Partly, masonry and especially unreinforced masonry (URM) has mechanical properties such as strength and ductility inferior to those of reinforced concrete and steel. Moreover, masonry structures were traditionally built based on rules of thumb acquired over many years of practice and/or empirical data from testing. Accordingly, we do not have a rigorous and uniform method of analysis and design for masonry. Nevertheless, the world still possesses numerous historic and ordinary masonry structures, which require maintenance and strengthening to combat the assault of time and nature. Hence, it is important to study fundamental properties of masonry so that new masonry structures can be effectively designed and built, and the cost for servicing old structures and for building new ones will be less expensive.

Mechanical Properties of Unreinforced Brick Masonry

Masonry is a heterogeneous composite in which brick units are held together by mortar. Brick units can be made from clay, compressed earth, stone or concrete. Mortar can be lime or a mixture of cement, lime, sand and water in various proportions. Consequently, masonry properties vary from one structure to the next depending on the type of brick units and mortar used. For each type of brick units and mortar, their properties depend upon the properties and composition of the constituents. Other factors contributing to the variability of masonry properties include anisotropy of units, dimension of units, mortar joint width, arrangement of bed-joints and head-joints, arrangement of brick units and workmanship. Nevertheless, bricks and mortar being the most visible components still determine the performance of masonry. Therefore, we should examine the properties of mortar and brick units in order to gain an insight into the behavior of masonry.

1.1 Properties of Mortar and Brick Units

Mortar is composed of cement and/or lime, sand and water. Properties of mortar vary depending on the proportions of these constituents. For instance, mortar with high water-cement (cementitious materials) ratio has lower compressive strength than low water-cement ratio. In order to standardize the practice, ASTM (American Standard Testing and Measurement) has designated four types of mortar for use in masonry construction in the United States. Table 1.1 lists the proportions and compressive strengths of the four types of mortar in accordance with ASTM 270.

Table 1.1: Volume proportions and compressive strength

Type	**Portland Cement**	**Hydrated Lime**	**Sand**	**Strength, psi (MPa)**
M	1	Min: 0, Max: 1/4	Not < 2-1/4 nor > 3 times sum of the total volume of cement and lime	2500 (17.2)
S	1	Min: 1/4, Max: 1/2		1800 (12.4)
N	1	Min: 1/2, Max: 1-1/4		750 (5.2)
O	1	Min: 1-1/4, Max: 2		350 (2.4)

Practically, the values given in Table 1.1 are only benchmarks for each type of mortar. The actual composition and strength can differ greatly from values given by ASTM. For instance, compression tests by McNary & Abrams (1985) on Type M (1:1/4:3 cement:lime:sand ratio and 1.83 water/cement ratio) and Type O (1:2:9 cement:lime:sand ratio and 0.51 water/cement ratio) give the average compressive strengths for 2-inch mortar cubes to be 7646 psi (52.6 MPa) and 498 psi (3.4 MPa), respectively. Type M mortar has higher compressive strength than Type O mortar as indicated in Table 1.1 and Figure 1.1.

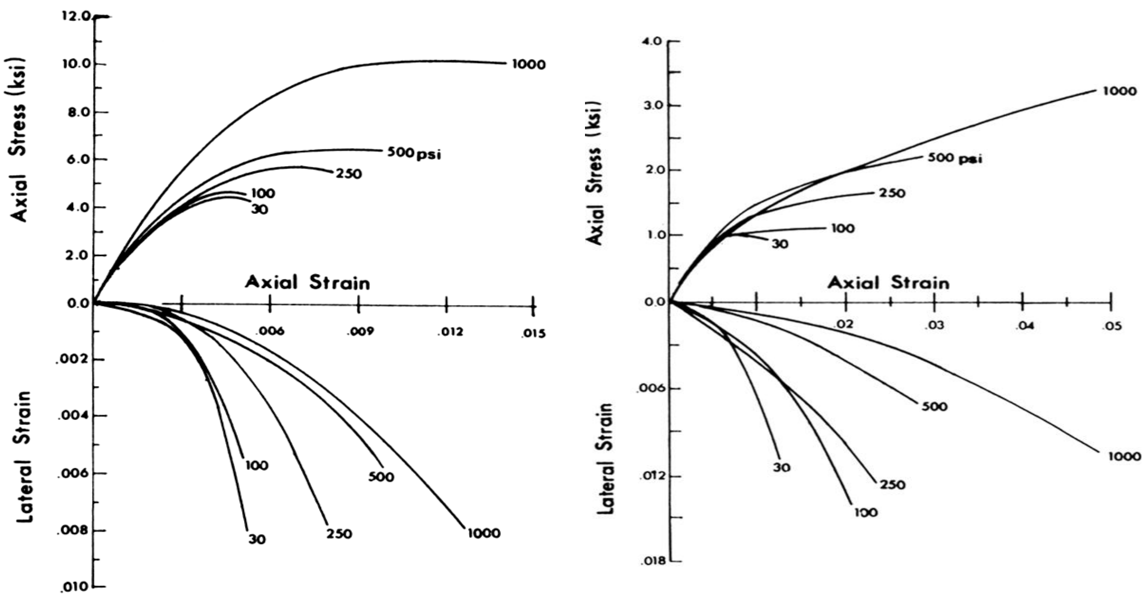

Type M **Type O**

Figure 1.1: Measured properties of types M and O mortars for different confining stresses [1.0 ksi = 6.90 MPa] (McNary & Abrams, 1985)

Moreover, experiments have shown that masonry prism under uniaxial compression perpendicular to bed joint, refer to Figure 1.4, produces tri-axial compression stress in the mortar. Under tri-axial compression, mortar behavior depends upon confining stresses and mortar type. Maximum crushing stress and strain increase with increase confining stresses. Also, lower strength mortars exhibit greater ductility than higher strength mortars. The plots of axial stress-axial strain and axial strain-lateral strain in Figure 1.1 for the two types of mortar clearly show that mortar exhibits nonlinear behavior under increasing confining pressure. Weaker mortar (Type O) exhibits greater axial shorting and lateral expansion than stronger mortar (Type M). Though, both strong and weak mortars exhibit brittle behavior at low confining stress. With regard to tensile strength of mortar, it is minimal and usually assumed to be zero.

Brick units also have many types and shapes. Although burned clay brick units seem to be ubiquitous around the world, there are other types of brick units such as unburned clay units, sand/clay mixed with cement, concrete units, calcium silicate bricks, and stone/rock. Similar to mortar, each type (SW: Severe weathering, MW: Moderate weathering, NW: No weathering, N: High strength and resistance to moisture penetration, S: moderate strength and resistance to moisture penetration) of brick units possesses its own properties. Table 1.2 lists the strengths for the three types of structural masonry units specified in ASTM.

Table 1.2: Compressive strengths of several types of bricks

ASTM C62: Clay or Shale bricks		
Type	Average compressive strength of 5 bricks	Compressive strength of 1 brick
SW	3000 psi (20.7 MPa)	2500 psi (17.2 MPa)
MW	2500 psi (17.2 MPa)	2200 psi (15.2 MPa)
NW	1500 psi (10.3 MPa)	1250 psi (8.6 MPa)
ASTM C55: Concrete bricks		
Type	Average compressive strength of 3 bricks	Compressive strength of 1 brick
N	3500 psi (24.1 MPa)	3000 psi (20.7 MPa)
S	2500 psi (17.2 MPa)	2000 psi (13.8 MPa)
ASTM C73: Calcium Silicate (Sand-Lime bricks)		
Type	Average compressive strength of 3 bricks	Compressive strength of 1 brick
SW	5500 psi (37.9 MPa)	4500 psi (31.0 MPa)
MW	3500 psi (24.1 MPa)	3000 psi (20.7 MPa)

In addition, a yield criterion for masonry units and uniaxial behavior of masonry units can be illustrated in Figure 1.2 according to Lofti & Shing (1994). Furthermore, mechanical properties of brick units such as clay units are directional in nature due to the extrusion process. Rad (1978) tested cylinders (0.667-in diameter by 1.3-in height) extracted from three faces of brick units and found that the variation in compressive strengths is as listed in Table 1.3. The same author also found that compressive strength of brick units on average is 2 to 3 times larger than the tensile strength.

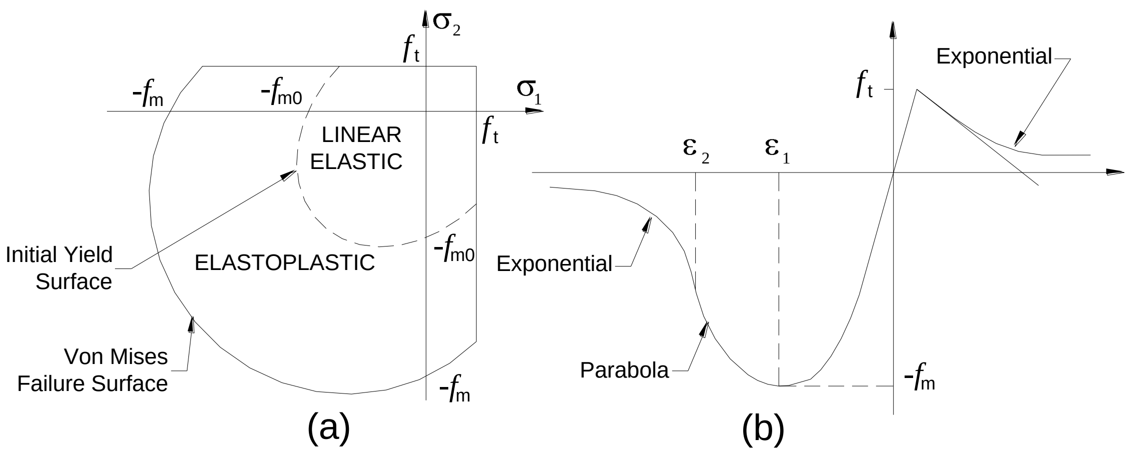

Figure 1.2: A yield criterion (a) and a typical stress-strain model (b) for brick unit (Lotfi & Shing, 1994)

Table 1.3: Directional compressive strength

Direction	Richtex brick	Southern brick
X (width of brick)	3042 ± 610	3140 ± 710
Y (length of brick)	5162 ± 822	6154 ± 2584
Z (direction of extrusion)	2475 ± 467	5089 ± 1369

Additionally, uniaxial compression tests of stack bonded masonry prisms show that brick units experience a compression-tension-tension state of stress. Since compressive strength of brick units is much stronger than tensile strength, brick units usually fail in tension. Biaxial compression-tension tests on brick by McNary & Abrams (1985) shows the interaction between compression (C) and tension (T) to fit the following relationship,

$$\frac{C}{C_0} = 1 - \left(\frac{T}{T_0}\right)^{0.58} \tag{1.1}$$

where C_0 and T_0 are uniaxial compressive strength and direct tensile strength, respectively. Khoo & Hendry (1973) also found such interaction between compression and tension in bricks tested under biaxial compression-tension. The concavity in the compression-tension interaction diagram, refer to Figure 1.3, is the indication of the interaction.

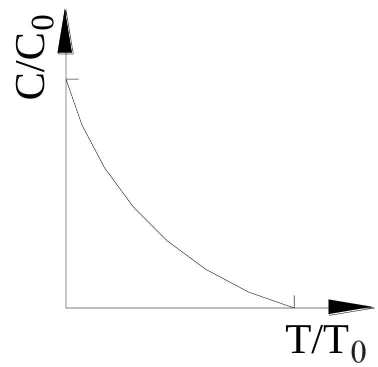

Figure 1.3: Interaction curve for bricks under biaxial compression-tension

1.2 Properties of Interface

The interface between a brick unit and a mortar joint is an important component of masonry. Being the weak link in masonry, interfaces usually dominate the behavior of masonry assemblage. Under certain load combinations such as pure tension normal to mortar joint and pure shear along mortar joint the interface controls the behavior of masonry. Tension and shear are the two different failure modes normally associated with unit-mortar interface.

1.2.1 Tension Mode

There are two types of bonds between mortar and brick units: chemical and friction. Tensile strength at the interface is primarily due to chemical bond. This bond depends upon the absorption rate of brick units. High absorption rate decreases the strength of the bond. Thus, brick units are usually wetted before they are laid. Direct tension and bending usually cause the bond to break, and where the break occurs we have separation of brick units and mortar layers. The tensile bond strength at the interface due to uniaxial tension and bending can be respectively calculated from,

$$f_t = \frac{F_u}{A_n} \tag{1.2}$$

$$f_{ft} = \frac{M_u}{S} \tag{1.3}$$

where F_u and A_n are ultimate axial force and net bonded area, respectively; M_u and S are bending moment at failure and elastic section modulus, respectively. The net bonded area is usually smaller than the cross-sectional area of the brick unit and concentrates in the middle of the unit. This is due to shrinkage of mortar and the process of laying units. Moreover, tensile failure at interface is brittle in nature. To capture the descending branch, Lourenco et al (1995) used the following expression which gives good approximation to the test results by Pluijm (1997),

$$\frac{\sigma}{f_t} = \exp\left(-\frac{f_t}{G_f^I} w_n \right) \tag{1.4}$$

where G_f^I and w_n are Mode-I fracture energy and crack band width in tension, respectively. Lourenco (1996) reported that the tensile fracture energy ranges from 0.005 N-mm/mm^2 (0.029 lbs-in/in^2) to 0.02 N-mm/mm^2 (0.11 lbs-in/in^2) for tensile bond strength ranging from 0.3 N/mm^2 (43.5 psi) to 0.9 N/mm^2 (130.5 psi). The fracture energy is defined as energy per net cracked area.

1.2.2 Shear Mode

Shear strength at the interface comes from friction due the asperities between the surface of mortar layer and the surface of the brick unit, and the chemical bond between mortar and brick units. Normal compression perpendicular to the interface further increases its shear strength because the asperities cannot easily slide over one another. Coulomb friction is often used to model this mode at the interface. Similar to the tension mode, formulation by Lourenco et al (1995) captures the descending branch under shear by the following expression,

$$\frac{\sigma}{c} = \exp\left(-\frac{c}{G_f^{II}} w_s \right) \tag{1.5}$$

where c, G_f^{II} and w_s are cohesion at interface, Mode-II (shear) fracture energy and crack width in shear, respectively. From Lourenco (1996), shear fracture energy is the area under the curve showing the relationship between shear displacement and residual dry friction shear level. This energy ranges from 0.01 N-mm/mm^2 (0.055 lbs-in/in^2) to 0.25 N-mm/mm^2 (1.43 lbs-in/in^2) for initial cohesion, *c*, values ranging from 0.1 N/mm^2 (14.5 psi) to 1.8 N/mm^2 (261 psi). This energy level increases linearly with increasing confining stress. Also, initial and residual internal friction angles can be measured from shear versus normal stress diagram. The initial ($\tan\phi_0$) ranges from 0.7 to 1.2 and residual ($\tan\phi_r$) is constant at 0.75. Dilatancy angle ($\tan\psi$), which measures the uplift of one unit over the other, ranges from 0.2 to 0.7; the value depends upon the roughness and confining stress. For either high pressure or increasing slip, $\tan\psi$ decreases to zero. Increasing slip grinds down the asperities at the interface, and increasing compression limits the uplift of brick units.

1.3 Behavior of Masonry under Uniaxial Compression

Previously, we have examined the properties of the components making up masonry. As we already know that masonry is a composite material composed of mortar, brick units and interfaces; thus, its properties are deemed to be different from those of each of its components. Now, we will examine mechanical properties of masonry as a composite.

1.3.1 Uniaxial Static Compression

Masonry is composed of two discrete entities: relatively stiffer masonry units and relatively softer mortar layers. They are chemically and physically bonded together. Under uniaxial compression, stacked masonry prism as shown in Figure 1.4 expands laterally in the plane perpendicular to the direction of loading. Yet, the stiffer masonry units expand less than the softer mortar, and restrain the expansion of mortar layers. As a result, masonry units experience a compression-bilateral tension state of stresses. At the same time, each mortar joint experiences a state of tri-axial compressive stresses. The in-plane compressive stresses in the mortar joint come from the restraining action by the stiffer masonry units.

Compressive strength of masonry under uniaxial compression depends chiefly on the tensile strength of the brick units. Nevertheless, Young's moduli and Poisson ratios of brick units and mortar, and thickness of mortar joints and brick units also play a role in the strength of the composite. Pande et al (1994) developed a sophisticate model for calculating the strength as follows,

$$f_m = \frac{f_t^b}{S_f} \cdot \frac{A_n}{A_g} \tag{1.6}$$

where S_f is a dimensionless stress factor as a function of elastic constants and thicknesses of mortar and bricks, f_t^b is tensile strength of brick unit, and A_n and A_g are net sectional area and gross area of the brick unit, respectively. The details for calculating f_m are in Pande et al (1994).

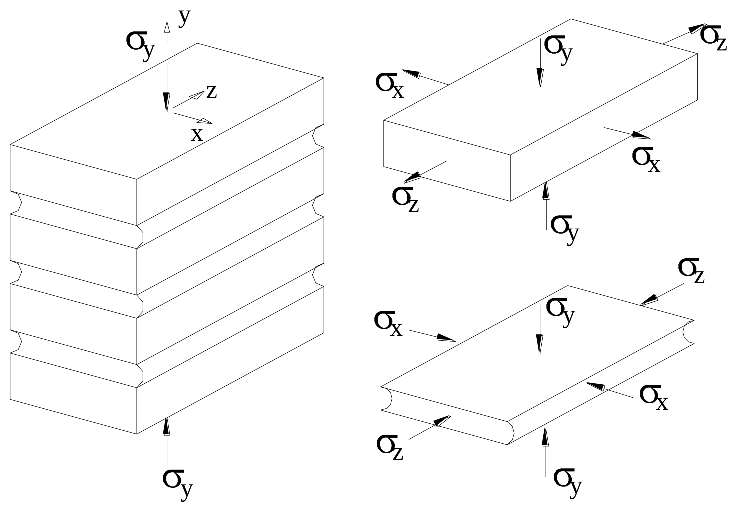

Figure 1.4: State of stresses in a masonry prism subjected to vertical compression

Experimentally, masonry prisms as observed by McNary & Abrams (1985) begin to spall at 85% of the ultimate load. Cracks form on the narrow faces of the prisms at 90% of the ultimate load. These cracks propagate and failure occurs with vertical splitting down the narrow face of the test prisms. Failure under uniaxial compression often begins in brick units due to its low tensile strength. The increment of stress inside brick units leading to failure , $\Delta\sigma_{b,x}$, can be computed as a function of the increment of vertical stress on the prism, $\Delta\sigma_y$, by the following expression from McNary & Abrams (1985),

$$\Delta\sigma_{b,x} = \frac{\Delta\sigma_y\left[\nu_b - \frac{E_b}{E_m(\sigma_1,\sigma_3)} \cdot \nu_m(\sigma_1,\sigma_3)\right]}{\left[1 + \frac{E_b}{E_m(\sigma_1,\sigma_3)} \cdot \frac{t_b}{t_m} - \nu_b - \frac{E_b}{E_m(\sigma_1,\sigma_3)} \cdot \frac{t_b}{t_m} \cdot \nu_m(\sigma_1,\sigma_3)\right]} \tag{1.7}$$

where subscripts b and m denote brick and mortar, respectively, ν is Poisson ratio, E is Young's modulus, and t is the thickness. It is noted that the mortar's Young modulus and Poisson ratio are functions of confining stresses.

Furthermore, failure modes under uniaxial compression also depend upon the type of mortar used. Strong mortars are usually associated with brittle and explosive failure; weak mortars are associated with ductile and slower rate of crack propagation. As mortar strength decreases, the stress-strain curve for the prism becomes more nonlinear. Meanwhile, brick strength has little influence on the nonlinearity of the stress-strain of the masonry prisms; the properties of brick are constant up to failure. This fact reflects upon the limited tensile strength of brick units and its brittleness. In short, the stress-strain of masonry depends primarily upon the properties of mortar beyond the linear range. Figure 1.5 clearly shows masonry prism built with Type O mortar has a greater nonlinearity than masonry prism built with stronger Type M mortar. Moreover, under uniaxial compression, average prism strength is almost equal to the average compressive strength of bricks and about 3 times greater than their tensile strength (Rad, 1978).

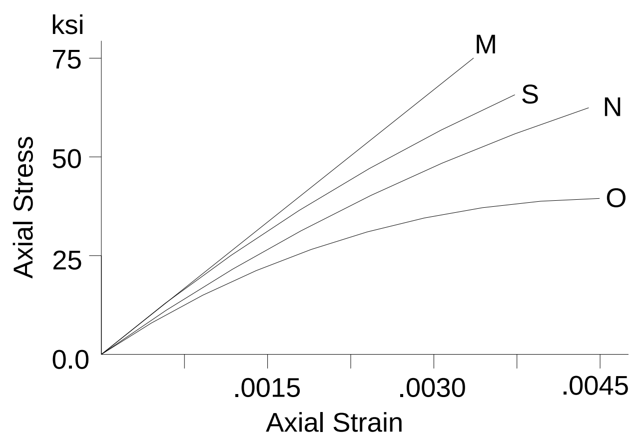

Figure 1.5: Stress-strain curves for prisms with different types of mortar (McNary & Abrams, 1985).

1.3.2 Behavior under Uniaxial Cyclic Compression

Compared to static loading, cyclic compression reduces brick masonry prisms compressive strengths by 30% (Naraine & Sinha, 1989). Under cyclic loading, stress-strain history of masonry prisms, according to Naraine & Sinha (1989) possesses a locus of common points and stability points. Common points are where the reloading portions of any loading cycles cross the unloading portions of the previous cycles; stresses above these points will produce additional strains, while stresses below will not and result in stress-strain path going into a loop where the point of intersection of the reloading curve and unloading curve descents and stabilizes at a lower bound called the stability point. The general form of stress-strain curves for common point and stability point under cyclic loading can be given as,

$$\sigma = \beta \frac{\varepsilon}{\alpha} \exp(1 - \varepsilon / \alpha) \tag{1.8}$$

where the stress, σ, and the strain, ε, are normalized values with respect the failure stress and the associated strain; β and α are constants. For loading perpendicular to the bed-joint, $\alpha = 0.85\beta + 0.15$ and for loading parallel to bed-joints, $\alpha = 0.77\beta + 0.23$. Table 1.4 gives the values of β for different curves and loading.

Table 1.4: Value of β for envelope, common point and stability point curves for uniaxial cyclic compression (Naraine & Sinha, 1989)

Loading case	Curve	Value of β
Perpendicular to bed-joints	Envelope Common-point Stability	1.00 0.84 0.65
Parallel to bed-joints	Envelope Common-point Stability	1.00 0.85 0.71

This empirically derived expression is for frog-clay brick unit of size 230 mm × 110 mm × 70 mm and 10 mm thick mortar joints. The strength of the brick unit was 13.1 N/mm^2 (1,900 psi), and 70-mm mortar cube was 6.1 N//mm^2 (885 psi). The loading rate was 2.9 N/mm^2 (421 psi) per minute and unloading was 5.8 N/mm^2 (841 psi) per minute. The plots of these curves are shown below in Figure 1.6.

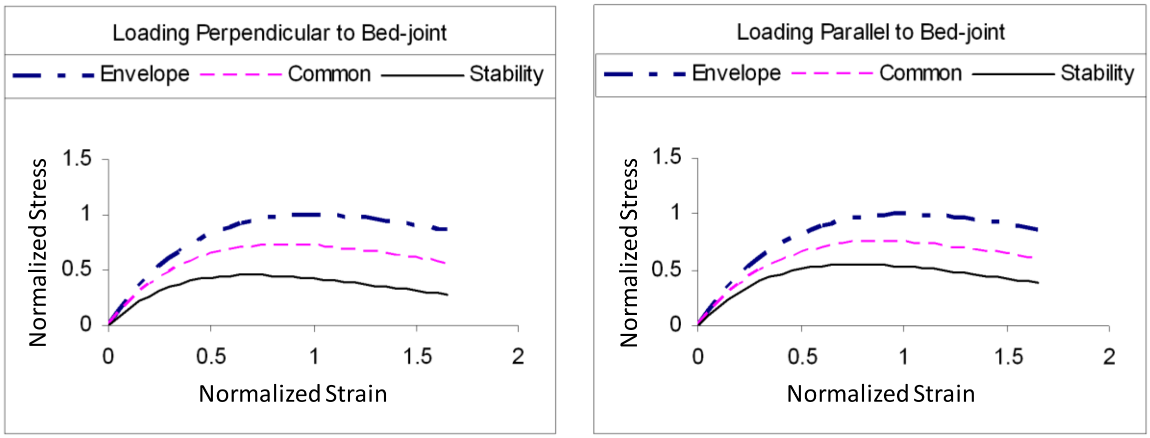

Figure 1.6: Stress-strain curves under uniaxial cyclic compression

In another similar experiment but with stronger "sand plast" (a type of calcium silicate) bricks with mean compressive strength of 23.4 N/mm^2 (3,394 psi), Alshebani & Sinha (1999) found cracks initiated at 55% and 45% of peak load perpendicular and parallel to bed-joints, respectively. The same types of failure modes as in the weaker clay brick specimens were observed. Also, the mathematical models for the envelope, common point and stability point curves still have the same forms as in weaker clay brick experiment by Naraine & Sinha (1989). For loading normal to bed-joints, the envelope stress-strain curve has the following form,

$$\sigma = \varepsilon^{\beta} \exp(1 - \varepsilon / \alpha) \tag{1.9}$$

On the other hand, for loading parallel to bed-joints, the envelope stress-strain curve has the following form,

$$\sigma = \varepsilon^{\beta} \exp\left[(1 - \varepsilon) \frac{\varepsilon}{\alpha + \beta} \right] \tag{1.10}$$

Common point and stability point stress-strain curves, for both loading normal and parallel to bed joints, have the following form,

$$\sigma = \varepsilon^{\beta} \exp[(1 - \varepsilon / \alpha)\varepsilon] \tag{1.11}$$

As before, the stress, σ, and strain, ε, are normalized values with respect to the average peak stress and strain. The constants α and β are determined from experimental data. Clearly, different types of bricks result in different expressions for stress-strain curves. However, an exponential stress-strain relationship in general fits the test data well.

Failure mode of brick masonry prisms varied according to the orientation of bed-joints. For specimens loaded perpendicular to bed-joints, failure was characterized by splitting of bricks in plane parallel to the plane of the prism and by formation of tensile cracks parallel to the axis of loading. For specimens loaded parallel to bed-joints, failure was characterized by splitting of bed-joints along the interfaces and some parallel cracks in the bricks. As an example from tests by Naraine & Sinha (1989), the mean failure stress for loading perpendicular to bed-joints was 5.40 N/mm^2 (783 psi) with standard deviation of 0.25 N/mm^2 (36 psi) and for loading parallel to bed-joints was 5.80 N/mm^2 (841 psi) with standard deviation of 0.30 N/mm^2 (44 psi). Moreover, the associated axial strains were $6.1\times10^{-3} \pm 3.4\times10^{-4}$ and $6.0\times10^{-3} \pm 4.0\times10^{-4}$, respectively.

1.4 Biaxial Behavior

Due to the variety of masonry, it is difficult to propose a truly general and representative stress-strain relationship in order to best describe masonry behavior. Testing is usually a preferred way to obtain behavior of the desired type of masonry. However, these tests are too specific for the types of masonry under investigation. Nevertheless, laboratory tests were performed by various researchers in an attempt to generalize the behavior of masonry under biaxial loading.

1.4.1 Biaxial Monotonic Behavior

Biaxial compression-compression and compression-tension tests are usually performed on masonry panels to obtain the stress-strain relationship. Dhanasekar et al (1985) performed tests on 180 half-scale brick masonry specimens, 360 mm (14.2 in) square. The brick dimensions were 110 mm × 50 mm × 35 mm (4.3 in × 2 in × 1.4 in). The mortar composition contained by volume 1 part cement, 1 part lime and 6 parts sand. Monotonically increasing load was applied to the specimens at an angle with respect to the bed-joint. In general, from the tests, most of nonlinear behavior is caused by the slippage at the mortar joints along the interfaces. These interfaces act as planes of weakness. Under compression-compression, tangent modulus changes as the load increases until failure. Under compression-tension, masonry fails elastically at low level of load; thus, masonry is considered to be linear elastic-brittle material when one of the principal stresses is tensile stress.

Furthermore, nonlinearity only occurs when masonry is under compression-compression state of stress. Initially, masonry behaves as a linear elastic material; therefore, masonry can be modeled, on average, as an isotropic continuum. From the experiment by Dhanasekar et al (1985), on an average, the value of elastic modulus in the direction normal to bed-joint is 5,600 MPa (813 ksi) with Poisson's ratio of 0.19; the value of elastic modulus in the direction parallel to bed-joints is 5,700 MPa (827 ksi) with Poisson's ratio of 0.19; the mean value of shear modulus is 2,350 MPa (341 ksi). These properties are also strongly influenced by the type of brick units used to construct the panel. Brick units with markedly directional properties will give rise to strongly orthotropic masonry. Beyond elastic range, Dhanasekar et al (1985) proposed Ramsberg-Osgood relationship to account for plastic strain,

$$\varepsilon = \frac{\sigma}{E} + \left(\frac{\sigma}{B}\right)^n \tag{1.12}$$

where *B* is constant with dimension of stress and *n* is dimensionless constant. Tests on 69 masonry panels give the values for *B* and *n* equal to 3.8 MPa (552 psi) and 3.1, respectively. Moreover, plastic strain is non-isotropic and related to joint directions. The authors found that for stress states $\sigma_n / \sigma_p \geq 0.25$ and $\tau / \sigma_n \leq 1$, the plastic strains normal to bed-joints, parallel to bed-joints and shear can be expressed as the powers of stresses normal to bed-joints (σ_n), parallel to bed joints (σ_p) and shear along the bed-joints (τ), respectively. These expressions are given in the following,

$$\left(\frac{\varepsilon_n^p}{\varepsilon_{n\gamma}}\right) = \left(\frac{\sigma_n}{B_n}\right)^{n_n} \tag{1.13a}$$

$$\left(\frac{\varepsilon_p^p}{\varepsilon_{p\gamma}}\right) = \left(\frac{\sigma_p}{B_p}\right)^{n_p} \tag{1.13b}$$

$$\left(\frac{\gamma^p}{\gamma_\gamma}\right) = \left(\frac{\tau}{B_s}\right)^{n_s} \tag{1.13c}$$

where $\varepsilon_n^p, \varepsilon_p^p, \gamma^p$ are normal, parallel and shear plastic strain components; $\varepsilon_{nr}, \varepsilon_{pr}, \gamma_r$ are reference strains; B_n, B_p, B_s are stress levels at which the reference strains were reached; and n_n, n_p, n_s are dimensionless constants in the power law. Table 1.5 gives the mean and coefficient of variation (COV) values of *n* and *B* (Dhanasekar et al, 1985),

Table 1.5: Constants in plastic stress-strain relationship

Direction	Mean *B* psi (MPa)	COV *B*	Mean *n*	COV *n*
Normal	1,060 (7.3)	0.19	3.3	0.29
Parallel	1,161 (8.0)	0.25	3.3	0.34
Shear	290 (2.0)	0.19	4.0	0.40

For stress state $\tau / \sigma_n > 1$, the bilinear stress-strain relationship is appropriate. Furthermore, the incremental form of plastic strain can be expressed as the ratio of incremental stress and the hardening modulus, *H*, as follows,

$$\delta\varepsilon^p = \frac{\delta\sigma}{H} \tag{1.14}$$

where *H* for each direction is given by,

$$H_n = 2{,}600\,(\varepsilon_n^p)^{-0.70} \text{ psi (i.e. } 17.9\,(\varepsilon_n^p)^{-0.70} \text{ MPa)} \tag{1.15a}$$

$$H_p = 2{,}860(\varepsilon_p^p)^{-0.70} \text{ psi (i.e.} 19.7(\varepsilon_p^p)^{-0.70} \text{ MPa)} \tag{1.15b}$$

$$H_s = 410\,(\gamma^p)^{-0.75} \text{ psi (i.e. } 2.8(\gamma^p)^{-0.75} \text{ MPa)} \tag{1.15c}$$

The above is for masonry made of solid pressed bricks. The model is not applicable to bricks with well defined directional properties or to mortar with strength closely matched to that of bricks.

1.4.2 Biaxial Cyclic Behavior

Unlike uniaxial compression, failure in the plane perpendicular to the plane of the panel is prevented by compression. Failure in the plane parallel to the free surface at mid-thickness, however, is not prevented. Failure is characterized by splitting of the panel into several columns. Naraine & Sinha (1991) found this type of failure in their test specimens when the following principal stress ratios (σ_n / σ_p = 0.2, 0.6, 1.0, 1.67 & 5.0, where σ_n is principal stress normal to bed-joint and σ_p is principal stress parallel to bed-joint) were applied to the specimens. Also, an average of 30% increase in dominant stress at failure was observed for the specimens under a low level of restraining stress. There was not observable increase in dominant stress at failure for high level of restraining stress. The authors found that a failure interaction curve can be expressed in terms of principal stress invariants and given as,

$$C J_2 + (1-C)I_1 + CI_2 = 1 \qquad (1.16)$$

where $J_2 = (\sigma_n / \sigma_{m\infty} - \sigma_p / \sigma_{m0})^2$, $I_1 = (\sigma_n / \sigma_{m\infty} + \sigma_p / \sigma_{m0})$, $I_2 = (\sigma_n \sigma_p / \sigma_{m\infty} \sigma_{m0})$; $\sigma_{m\infty}$ and σ_{m0} are average uniaxial compressive strengths normal and parallel to bed-joint, respectively. *C* is a constant governing the nature of interaction; for *C* =1.0, the equation reduces to Von Mises criterion; from the experiment, the authors found *C* =1.6. The stress-strain relationship of the panel is governed by critical principal strain and the associated stress. The principal strain ratios ($\varepsilon_n / \varepsilon_p$) are linear up to failure. For small σ_n / σ_p ratios, ε_n changes very insignificantly until failure; similarly for ε_p when σ_n / σ_p is large. The stress-strain curve can be expressed as following,

$$\sigma = \beta \frac{\varepsilon}{\alpha} - \exp\left(1 - \frac{\varepsilon}{\alpha}\right) \qquad (1.17)$$

The constants α and β are parameters representing envelope curves, which are stress-strain curves obtained from monotonically increasing load, not cyclic loading. The constants can be determined by least square method in combination with test data. The stress-strain for envelope curves has the following form,

$$\sigma = \varepsilon * \exp(-\varepsilon) \qquad (1.18)$$

In the above equations, the stress and strain are normalized with the critical stress and strain given in Tables 1.6 and 1.7. The constants α and β are linearly related and given in Table 1.8.

Table 1.6: Critical stress-strain parameters perpendicular to bed-joint

σ_n/σ_p	Mean σ_{mn} (N/mm^2)	COV σ_{mn}	Mean ε_{mn}	COV ε_{mn}
∞	6.10	0.05	0.0065	0.08
5.00	8.02	0.07	0.0060	0.09
1.67	8.32	0.08	0.0054	0.11
1.00	8.10	0.07	0.0043	0.11

Table 1.7: Critical stress-strain parameters parallel to bed-joint				
σ_n/σ_p	Mean σ_{mn} (N/mm^2)	COV σ_{mn}	Mean ε_{mn}	COV ε_{mn}
0.0	6.70	0.08	0.00580	0.15
0.2	8.65	0.07	0.00545	0.13
0.6	8.84	0.07	0.00490	0.12

Table 1.8: Values of α, β, i_c (degree of fit between experimental and theoretical)							
σ_n/σ_p	Expression for α	Envelope vurve		Common point		Stability point	
		β	i_c	β	i_c	β	i_c
0.00	$0.78\beta + 0.22$	1.0	0.95	0.87	0.95	0.68	0.85
0.20	$0.59\beta + 0.41$	1.0	0.96	0.83	0.94	0.65	0.93
0.60	$0.88\beta + 0.12$	1.0	0.95	0.85	0.93	0.69	0.94
1.00	$0.68\beta + 0.32$	1.0	0.96	0.84	0.96	0.64	0.95
1.67	$0.79\beta + 0.21$	1.0	0.95	0.83	0.95	0.66	0.95
5.00	$0.62\beta + 0.38$	1.0	0.94	0.83	0.95	0.68	0.93
∞	$0.89\beta + 0.11$	1.0	0.97	0.88	0.92	0.71	0.94

The plastic strain normalized to the critical value is given by,

$$\varepsilon_r = a\varepsilon^2 + b\varepsilon \tag{1.19}$$

where constants *a* and *b* are given in Table 1.9.

Table 1.9: Values of a and b for plastic strain									
σ_n/σ_p	ε_r vs. ε_E (Envelope)			ε_r vs. ε_C (Common)			ε_r vs. ε_S (Stability)		
	a	b	i_c	a	b	i_c	a	b	i_c
0.00	0.240	0.150	0.96	0.250	0.150	0.90	0.250	0.220	0.94
0.20	0.270	0.122	0.95	0.254	0.146	0.96	0.340	0.084	0.96
0.60	0.292	0.095	0.96	0.301	0.101	0.97	0.395	0.029	0.95
1.00	0.312	0.110	0.95	0.318	0.108	0.94	0.443	0.071	0.96
1.67	0.304	0.132	0.95	0.320	0.127	0.96	0.386	0.118	0.96
5.00	0.302	0.126	0.96	0.332	0.116	0.96	0.323	0.175	0.97
∞	0.270	0.170	0.96	0.270	0.181	0.95	0.340	0.151	0.95

Alshebani & Sinha (2000) performed the same experiment with stronger bricks (sand-plast, a type of calcium silicate) and with principal stress ratios, σ_n / σ_p = 0.25, 0.50, 1.0, 2.0 & 6.0. The mean compressive strength of bricks was 23.4 N/mm^2 (3,394 psi). The same type of failure (splitting at mid-thickness) was observed. However, reflecting the difference in compressive strength between sand-plast brick and clay brick, the analytical expressions for failure interaction curve, envelope curve, common-point curve, and stability-point curve are different. Though still a function of principal stress invariants, the failure interaction curve is expressed as follows,

$$X_1 J_2 + (1 - X_1) I_1 + X_1 I_2 = 1 \tag{1.20}$$

where $J_2 = (\sigma_n / \sigma_{m\infty} - \sigma_p / \sigma_{m0})^2$, $I_1 = (\sigma_n / \sigma_{m\infty} + \sigma_p / \sigma_{m0})$, $I_2 = (\sigma_n \sigma_p / \sigma_{m\infty} \sigma_{m0})$, and $X_1 = (1 - \sigma_p / \sigma_n)$. X_1 is equal to 1.0 for uniaxial loading. For envelope curve normal to bed-joints,

$$\sigma = \varepsilon^{\beta} \exp(1 - \varepsilon / \alpha) \tag{1.21}$$

For envelope curve parallel to bed-joints,

$$\sigma = \varepsilon^{\beta} \exp\left[(1 - \varepsilon) \frac{\varepsilon}{\alpha + \beta} \right] \tag{1.22}$$

For common-point and stability-point,

$$\sigma = \varepsilon^{\beta} \exp\left[(1 - \frac{\varepsilon}{\alpha}) \varepsilon \right] \tag{1.23}$$

Again, σ and ε are non-dimensional stress and strain, normalized by the critical stress and strain, respectively. Tables 1.10 and 1.11 list the values for the critical stress and strain and the constants α and β.

Table 1.10: Critical stress-strain parameters

σ_n/σ_p	σ_{mn} (N/mm^2)	ε_{mn}	σ_{mp} (N/mm^2)	ε_{mp}
∞	9.5	5.2×10^{-3}	None	None
4.00	12.0	4.9×10^{-3}	None	None
2.00	12.4	4.5×10^{-3}	None	None
0.00	None	None	8.2	5.7×10^{-3}
0.25	None	None	11.2	5.4×10^{-3}
0.50	None	None	12.1	5.0×10^{-3}
1.00	None	None	11.8	4.3×10^{-3}

Table 1.11: Values for α, β and i_c

σ_n/σ_p	Envelope curve			Common point curve			Stability point curve		
	α	β	i_c	α	β	i_c	α	β	i_c
0.00	0.73	0.70	0.96	0.70	0.73	0.92	0.54	0.73	0.89
0.25	0.73	0.70	0.94	0.66	0.78	0.94	0.50	0.76	0.93
0.50	0.73	0.70	0.94	0.65	0.76	0.93	0.49	0.76	0.92
1.00	0.73	0.70	0.96	0.63	0.78	0.95	0.47	0.76	0.90
2.00	1.00	1.00	0.93	0.69	0.81	0.92	0.54	0.85	0.91
4.00	1.00	1.00	0.91	0.70	0.82	0.92	0.54	0.82	0.88
∞	1.00	1.00	0.97	0.73	0.80	0.95	0.58	0.80	0.90

Furthermore, it is important to recognize that properties of brick masonry prisms vary depending on the type of bricks used, joint geometry and workmanship.

1.5 Shear Behavior

Peak shear resistance depends upon mortar type, mortar water/cement ratio, brick surface structure as measured by initial rate of absorption (IRA) and workmanship (Atkinson et al, 1989). Under direct shear tests, shear distribution is uniform along bed joints for specimens subjected to unit shear and zero normal loads. Plot of shear load versus relative shear displacement (Figure 7) from direct shear test experiments by Atkinson et al (1989) shows a very steep ascend to peak value and a steep descend to residual value in the first cycle, and shows no secondary peak after the first cycle. Yet, for the case of low normal load, a secondary peak can be observed upon shear reversal of the first cycle. The residual shear strength after first cycle does not seem to be affected by the number of cycles. Moreover, in the first cycle softening in bed-joints can be seen as indicated in the decrease of slope before peak shear. Also, bed-joints dilate and contract twice per cycle. Except for cases of low normal load levels, the net result of shearing is contraction; dilatation part is insignificant under medium and high normal load levels. Vertical deformation in bed-joints is small and elastic.

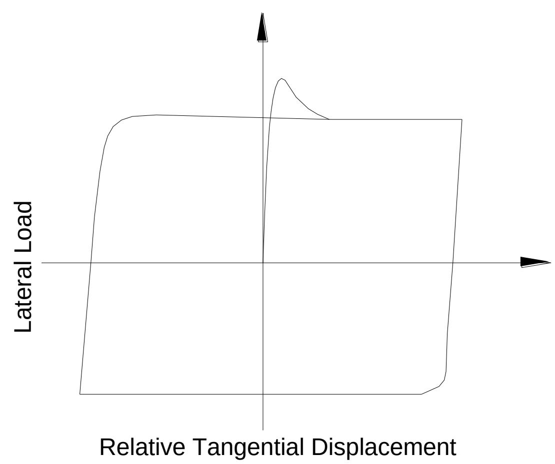

Figure 1.7: An example of shear stress-strain relationship

To represent the peak and residual shear strengths, the following Mohr-Coulomb criterion was found to be well matched by Atkinson et al (1989).

$$\tau = c + \sigma_n \tan\phi \qquad (1.24)$$

The parameters c and $\tan\phi$ can be evaluated by regression analysis. The parameter $\tan\phi$ ranges from 0.7 to 0.85. Table 1.12 gives the values for c and $\tan\phi$ from the tests by Atkinson et al (1989).

Table 1.12: Results of linear regression on direct shear test data (Goodness of fit=R^2_p)

Specimen type (number of tests)	Peak values (MPa)			Residual values (MPa)		
	$\tan\varphi_p$	c_p	R^2_p	$\tan\varphi_r$	c_r	R^2_r
Old bricks and 1:2:9 mortar, 7 mm (9)	0.640	0.213	0.995	0.693	0.038	0.996
Old bricks and 1:2:9 mortar, 13 mm (16)	0.695	0.127	0.994	0.678	0.023	0.995
New bricks and 1:1.5:4.5 mortar, 7 mm (9)	0.745	0.811	0.985	0.747	0.037	0.999

For shear stiffness, the following empirical model for nominal shear stress and the relative displacement (u) can be used,

$$\tau = \frac{u}{a + bu} \qquad (1.25)$$

where a and b are parameters obtained by fitting experimental data and in general they vary with the normal stress level. The shear stiffness is given by,

$$k_s = \frac{\partial \tau}{\partial u} \qquad (1.26)$$

The constant, a, is reciprocal of the initial bed-joint shear stiffness (=$1/k_{si}$), and $1/b$ is horizontal asymptote to the hyperbolic τ-u curve. Table 1.13 gives the expressions for a and b in the experiment by Atkinson et al (1989).

Table 1.13: Expressions for a and b

Specimen type	Regression on a	Regression on $1/b$
Old clay units 1:2:9, 7mm	$a = 0.054 - 0.005\sigma_n$	$1/b = 0.166 - 0.976\sigma_n$
Old clay units 1:2:9, 13 mm	$a = 0.065 - 0.001\sigma_n$	$1/b = 0.457 - 0.762\sigma_n$
New clay units 1:1.5:4.5, 7 mm	$a = 0.046 - 0.004\sigma_n$	$1/b = 0.808 - 1.231\sigma_n$

1.6 Conclusion

In this chapter, we have investigated the mechanical properties of masonry from experiments by various researchers. Masonry is a composite material of brick units and mortar joints and interface between mortar and unit. Together, they determine the properties of masonry. The interface is known as the weak link in the system with minimal tensile bond strength, thus masonry has limited tensile strength and usually negligible. Under uniaxial compression, state of stresses in the brick in a masonry prism is compression-tension-tension; whereas, softer mortar joint is under tri-axial compression. Under tension, masonry is linear elastic material; tensile failure is characterized by splitting along the interface. Masonry exhibits nonlinearity under biaxial loading. Cyclic loading reduces compressive strength of masonry prism by 30%. Shear behavior of masonry depends upon normal stress; under high normal stress, dilatancy is insignificant. Mohr-Coulomb model is appropriate for modeling shear behavior in joint.

References

1. AlShebani, M. M. & Sinha, S. N. (1999), "Stress-Strain Characteristics of Brick Masonry Under Uniaxial Cyclic Loading," *Jr. of Structural Engineering,* June 1999, pp. 600-604.
2. AlShebani, M. M. & Sinha, S. N. (2000), "Stress-Strain Characteristics of Brick Masonry under Cyclic Biaxial Compression," *Jr. of Structural Engineering,* June, pp. 1004-1007.
3. Andreaus, U. (1996), "Failure Criteria for Masonry Panels under In-Plane Loading," *Jr. of Structural Engineering,* January 1996, pp. 37-46.
4. Atkinson et al (1989), "Response of Masonry Bed-Joint in Direct Shear," *Jr. of Structural Engineering*, 115(9), pp. 2276-2296.
5. Bruneau, M. (1995). "Damage to Masonry Buildings from the 1995 Hanshin-Awaji (Kobe, Japan) Earthquake," *Proc. Of the 7th Canadian Masonry Symposium,* Vol. 1, pp. 84-98.
6. Costley, A. C. and Abrams, D. P. (1995). "Seismic Response of URM Buildings," *Proc. Of the 7th Canadian Masonry Symposium,* Vol. 1, pp. 72-83.
7. Dhanasekar et al (1985), "Biaxial Stress-Strain Relations for Brick Masonry," *Jr. of Structural Engineering*, 111(5), pp. 1085-1100.
8. Drysdale, R. G. & Essawy, A. S. (1988), "Out-of-Plane Bending of Concrete Block Walls*," Jr. of Structural Engineering*, 114(1), pp. 121-133.
9. El-Dakhakhni, W. W., M. Elgaaly & A. A. Hamid (2003). "Three-Strut Model for Concrete Masonry-Infilled Steel Frames," *Jr. of Structural Engineering*, 129(2), pp. 177-185.
10. Gazzola, E. & Drysdale, R. G. (1986), "A Component Failure Criterion for Blockwork in Flexure," New Analysis Techniques for Structural Masonry, ed. S. C. Anand.
11. Giordano, A., E Mele & A. De Luca (2002). "Modeling of Historical Masonry Structures: Comparison of Different Approaches through a Case Study," *Engineering Structures*, 24, pp. 1057-1069.

12. Khoo, C. L. & Hendry, A. W. (1973), "A failure Criteria for Brickwork in Axial Compression," *Proceedings*, Third International Brick and Masonry Conference, Essen, Germany, pp. 139-145.
13. Lourenco, P. B., Rots, J. G. & Blaauwendraad, J. (1995), "Two Approaches for the Analysis of Masonry Structures: Micro and Macro-Modeling," *HERON*, 40(4), pp. 313-340.
14. Lourenco, P. B. (1996), <u>Computational Strategies for Masonry Structures</u>, Ph.D. Thesis.
15. Lourenco, P. B. (2000), "Anisotropic Softening Model for Masonry Plates and Shells," *Jr. of Structural Engineering*, 126(9), pp. 1008-1016.
16. Lotfi, H. R. & P. B. Shing (1994), "Interface Model Applied to Fracture of Masonry Structures," *Jr. of Structural Engineering*, 120(1), pp. 63-80.
17. Magenes, G. & G. M. Calvi (1997), "In-Plane Seismic Response of Masonry Walls," *Earthquake Eng. & Struct. Dynamics*, 26, pp. 1091-1112.
18. Mahmoud, A. D. S., Hamid, A. A. & Magd, S. A. E. (1995). "Lateral Response of Unreinforced Solid Masonry Shear Walls: An Experimental Study," *Proc. Of the 7th Canadian Masonry Symposium*, Vol. 1, pp. 110-125.
19. McNary, W. S. & D. P. Abrams (1985), "Mechanics of Masonry in Compression," *Jr. of Structural Engineering*, pp. 857-870.
20. Mosalam, K.M., "Mechanical Properties and FE Modeling of Concrete Block Masonry and its Constituents," *Proc. 2001 Second International Conference on Engineering Materials*, Vol. 1, 421-432, San Jose, CA, USA, 2001.
21. Naraine, K. & Sinha, S. N. (1989), "Behavior of Brick Masonry under Cyclic Compressive Loading," *Jr. of Structural Engineering*, pp. 1432-1445.
22. Naraine, K. & Sinha, S. N. (1991), "Cyclic Behavior of Brick Masonry under Biaxial Compression," *Jr. of Structural Engineering*, 117(5), pp. 1336-1355.
23. Page, A. W., Peter W. Kleeman & Manicka Dhanasekar (1985), "An In-Plane Finite Element Model for Brick Masonry," in <u>New Analysis Techniques for Structural Masonry</u>, edited by S. C. Anand.
24. Pande et al (1989), "Equivalent Elastic Moduli for Brick Masonry," *Computers and Geotechnics*, 8, pp. 243-265.

25. Pande, G. N., B. Kralj & J. Middleton (1994), "Analysis of the Compressive Strength of Masonry Given by the Equation $f_k = K(f_b')^{\alpha}(f_m)^{\beta}$," *The Structural Engineer*, 71(1), pp. 7-12.
26. Pietruszczak, S. & X. Niu (1992). "A Mathematical Description of Macroscopic Behavior of Brick Masonry," Int. J. Solids Structures, 29(5), 531-546.
27. Pluijm, R. van der (1997), "Non-linear Behavior of Masonry under Tension," *HERON*, 42(1), pp. 25-55.
28. Rahman, M. A. & Anand, S. C. (1994), "Empirical Mohr-Coulomb Failure Criterion for Concrete Block-Mortar Joints," *Jr. of Structural Engineering,* 120(8), pp. 2408-2422.
29. Salamon, M.D.G. (1968), "Elastic Moduli of A Stratified Rock Mass," *Int. J. Rock Mech. Min. Sci.*, 5, pp. 519-527.
30. Schellekens, J. C. J. & R. de Borst (1990), "The Use of Hoffman Yield Criterion in Finite Element Analysis of Anisotropic Composite," Computers & Structures, 37(6), pp. 1087-1096.
31. Sucuoglu, H. & Erberik, A. (1997). "Performance Evaluation of A Three-Storey Unreinforced Masonry Building During the 1992 Erzincan Earthquake," *Earthquake Eng. and Struct. Dynamic*, 26 (3), pp. 319-336.
32. Tomazevic, M. (1987). "Dynamic Modelling of Masonry Buildings: Storey Mechanism Model as A Simple Alternative," *Earthquake Eng. and Struct. Dynamics*, 15, pp. 731-749.
33. Tomazevic, M. & Weiss, P. (1994). "Seismic Behavior of Plain- and Reinforced-Masonry Buildings," *Jr. of Structural Engineering,* 120(2), pp. 323-338.
34. Yokel, F. Y. & S. G. Fattal (1976). "Failure Hypothesis for Masonry Shear Wall," *Jr. of Structural Engineering*, 120(ST3), pp. 515-532.